The growth of bilayer defects and the induction of interdigitated domains in the lipid-loss process of supported phospholipid bilayers

Ye Fang, Jie Yang *

Physics Department, University of Vermont, Cook Building, Burlington, VT 05405, USA

Abstract

The lipid-loss process has been studied with in situ atomic force microscopy (AFM) at six different temperatures for supported dipalmitoylphosphatidylcholine (DPPC) bilayers. A typical structural characteristic is the creation and the growth of bilayer defects as lipid molecules are lost from the bilayer. The rate of the lipid loss has an Arrhenius behavior, with an activation energy of 37 kT, where kT is the thermal energy at room temperature. For the lipid-loss processes at temperatures above 45°C, interdigitated membrane domains are induced and are mostly in contact with some bilayer defects. These domains disappear at the increase of the area of bilayer defects. Possible mechanisms of these phenomena are discussed.

Keywords: Supported membrane; Atomic force microscopy; Phospolipid; Lipid interdigitation

1. Introduction

The lipid bilayer is basic structural framework of biological membranes. It houses membrane proteins such as channels and ion-pumping ATPases and membrane receptors which regulate various cellular and sub-cellular functions and activities [1–4]. In order to understand the properties of biological membranes, it is therefore of great importance to study the basic structural framework, the lipid bilayer. For this purpose, model phospholipid membranes have been widely used [5,6]. The use of model membranes made of single component has the advantage of simplification. Thus complicated biological processes in membranes of living organisms can be analyzed stepwise. One prominent characteristic of lipid bilay-

ers is the dynamic nature of lipids in the bilayers. Thus far, extensive studies on the dynamic properties of phospholipids have revealed much information about the organization and the function of these lipids in biological membranes [7,8]. Thermodynamically, free monomeric lipid molecules coexist with lipid bilayers in aqueous solution [9,10], although the population of the former is much less, as a result of the hydrophobic interaction between lipid molecules which drives the assembly of lipid bilayers [11]. Light scattering measurements and uses of fluorescent, radioactive, and spin labels have facilitated the study of the lipid-exchange process and have shown that it has a rather long thermal equilibrium time, with a time constant of the order hours around 37°C [12–19]. The lipid-exchange process involves the transfer of monomeric lipid molecules from the bilayer to the solution and vice versa. The rate of the

---

* Corresponding author. Fax: + 1 (802) 656 0817.

lipid exchange has an Arrhenius behavior, with a barrier in the range of 30–50 kT, where kT is the thermal energy at room temperature [15–18]. These results are obtained from averages of large ensembles and thus are insensitive to any information regarding local inhomogeneities. Such inhomogeneities, however, may play an important role in the molecular level lipid-exchange processes.

Most cells in living organisms are anchored to some kind of matrices and thus are partially supported [1,20,21]. Therefore, studies of supported membranes are also of biological relevance [22]. Supported model bilayers have been used to study cell–cell recognition processes [23,24], antibody–antigen interactions [25,26], and enzymatic characteristics of blood coagulation cascade [27,28]. Supported membranes are also widely used as biosensors [22]. The advent of atomic force microscope (AFM), with its capability of operating in solution [29], allows the probing of local structural details of supported membranes at high resolution [30–36]. With the AFM, supported bilayers can also serve as substrates to facilitate in situ structural determination of membrane proteins at high resolution, and to study protein–membrane interactions [35,37–43]. Therefore, it is possible now to correlate functional studies to local variations in supported membranes. Specifically, the dynamic process of the lipid-exchange process can be studied by measuring the loss of lipids and monitoring accompanying structural changes in bilayers.

Here, we report AFM studies of the lipid-loss process in supported bilayers. The loss of lipids is characterized by the increase of defect areas. Measurements of defect areas from a large number of AFM images provide better statistics in calculating the lost amount of lipids in the bilayers. We have found some interesting structural features associated with the lipid-loss process. Interdigitated membrane domains are induced in the lipid-loss process at temperatures above 45°C and disappear at later times as the area of bilayer defects increases. Most of these domains are in contact with some bilayer defects. The rate of the lipid loss is extremely slow and has an Arrhenius behavior with an activation energy of 37 kT. We sometimes observe some circular structures on the substrate as most lipid molecules leave the bilayer. Possible mechanisms of these phenomena are discussed.

2. Materials and methods

2.1. Materials and specimen preparation

Dipalmitoylphosphatidylcholine (DPPC) lipids in the powder form were obtained from Sigma (St. Louis, MO) and used without further purification. Small unilamellar vesicles were prepared by sonicating fresh lipid suspension until clear [44,45], using a Fisher FS3 ultrasonic cleaner. The suspension, about 0.5 mg/ml of lipids in 20 mM NaCl, is in a glass culture tube, which was sealed by several layers of parafilms after purging the air with nitrogen gas. The optically transparent suspension was then centrifuged at 14 000 rpm for about 30 min. The supernatant was used. Specimens of supported unilamellar bilayers were prepared by the vesicle-fusion method as previously reported [23,32]. Briefly, a drop of about 200 μl of the lipid suspension was applied to a piece of freshly cleaved mica ($\approx 3 \times 5$ mm^2), allowing incubation at 4°C overnight. The mica was attached to the 1.6-cm diameter metal disk supplied by Digital Instruments (Santa Barbara, CA). A silicon rubber O-ring was placed on the metal disk enclosing the piece of mica. After the incubation, a drop of 20 mM NaCl of about 100 μl was applied to the mica to dilute the concentration of the vesicles. The O-ring keeps the droplet within its boundary. The surface tension prevents any leaking of the solution from the bottom of the O-ring. Sometimes, vacuum grease was applied to the O-ring to strengthen the adhesion of the O-ring to the metal disk. The substrate was heated for about 30 min at 50°C. Afterwards, about 20 exchanges with 200 μl of 20 mM NaCl solution were made to remove excess vesicles from the droplet. The specimen was imaged by the AFM to check for the membrane.

2.2. AFM imaging

A NanoScope E AFM and oxide-sharpened Si$_3$N$_4$ tips with a nominal spring constant of 0.06 N/m, all from Digital Instruments (Santa Barbara, CA), were used in this work. All images were obtained under a probe force of about 0.5 nN in the contact mode, at a pixel number of 512×512, and with a scanning line speed of about 5 Hz. A home-made fluid cell was used for imaging in solution. The piezo scanner we
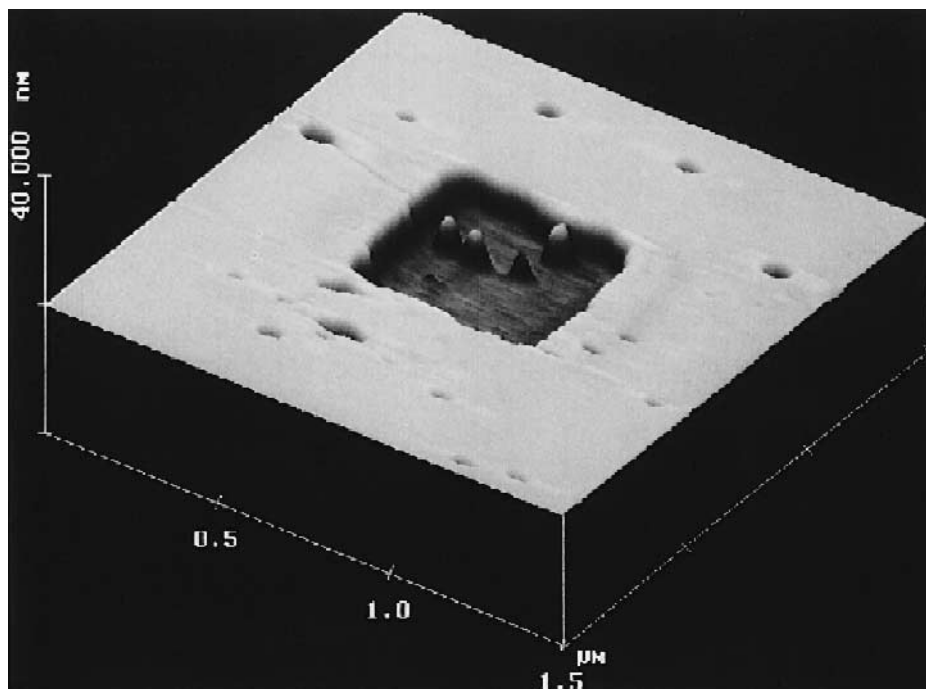
Fig. 1. A supported unilamellar bilayer of DPPC in surface plot to show the 3-D perspective of the planar structure. The bilayer was in 20 mM NaCl at room temperature (about 23°C).

used has a scanning range of 10 μm. Fig. 1 shows an AFM image of a supported DPPC bilayer in the surface plot to demonstrate the 3-D perspective of the planar structure. The thickness of the bilayer is about 6 nm. The square defect was created by AFM tip at a probe force of about 10 nN, a scanning line speed of 244 Hz, and a scanning window of 0.49 μm^2. The image is presented in a layered gray scale to show the substrate in the defect area. In the layered gray scale, as the height of imaged objects changes from high to low, the brightness of the image varies from bright to dark and then back to bright again. Thus, the substrate can be adjusted visible. In a normal gray scale, the brightness changes from bright to dark monotonically as the height of imaged objects changed from high to low. A drawback with the normal gray scale is that the substrate can be totally dark and thus invisible when imaged objects are relatively high. It appears that the layered gray scale provides a better 3-D perspective of the planar bilayer structure.

2.3. Characterization of the loss of lipids

In conventional methods, the study of the lipid-exchange process usually proceeds by introducing an imbalance and recording how the system reaches the equilibrium [15,17,18]. In thermal equilibrium, we have [9,10],

$$\mu_{W} - \mu = -\mathrm{RT} \ln x_{W} \tag{1}$$

where μ is the chemical potential of lipids in the bilayer, μ_{W} is the chemical potential of lipids in the solution, RT is the molar thermal energy, and x_{W} (< 1) is the concentration of lipids in solution. The difference in the chemical potentials between lipids in the two media stabilizes the lipid bilayer in solution. Thus, an Arrhenius behavior for the lipid-exchange process is expected, as demonstrated in experiments on vesicular systems [15–18]. For a supported bilayer, incubating it with a large volume of lipid-free solution should cause the loss of lipids as a result of reaching thermal equilibrium of the bilayer with its surrounding environment. Therefore, in supported bilayers, the lipid-loss process is equivalent to the lipid-exchange process. With the AFM, the lipid-loss process can be studied by measuring areal increase of bilayer defects. The probe of local structure, the high-resolution of the AFM, and the imaging in solution may allow direct observation of where in the

bilayer the lipid loss occurs. In our experiments, original bilayers are examined with the AFM. For any bilayer that has a low percentage of bilayer defects, the specimen is taken out of the AFM cell and is transferred to a small petri-dish filled with lipid-free solution (about 9 ml 20 mM NaCl). The petri-dish is then heated to a certain temperature for a given time. Afterwards, the bilayer is cooled back to room temperature and examined again by AFM to detect the defect-areal increase. After taking the metal disk out of the petri-dish, the supported bilayer that was immersed in a drop of about 200 μl solution was cooled back to room temperature under ambient condition within several minutes.

Since all AFM experiments were performed at room temperature, any lipid loss at room temperature causes counting error in determining the lipid-loss rate for those incubation temperatures above room temperature. Fortunately, we found that the lipid-loss rate at room temperature is much slower than those at higher temperatures. Thus, the error is within our experimental precision. For the same reason, we cannot obtain the lipid-loss rate for temperatures lower than room temperature.

2.4. Measurements of bilayer defects

AFM images store digitized data that greatly facilitate the measurement of bilayer defects. In each AFM image, there are 512 scanning lines, with each line containing 512 data points. In a bilayer image, the bilayer is planar and defects are lower in the vertical z-direction by a bilayer thickness. The defect area is determined by counting those data points with lower vertical z-values. For this purpose, it is preferable to image an area as large as possible. However, the piezo response is not quite linear at larger scanning sizes. Some instrumental electronic noises or drifts are also shown in larger area scans. All these contribute to some variation in the detector signal which results in a modulation in the z-value. An example is shown in Fig. 2a in which the scanning line demonstrates a bilayer with three defects. Here, 512 points are rounded off to 256 points. Such a round off reduces greatly the analysis time, and should not affect any significantly the determination of the defect coverage percentage. The slow modulation in z-direction is not due to the structure of bilayer.
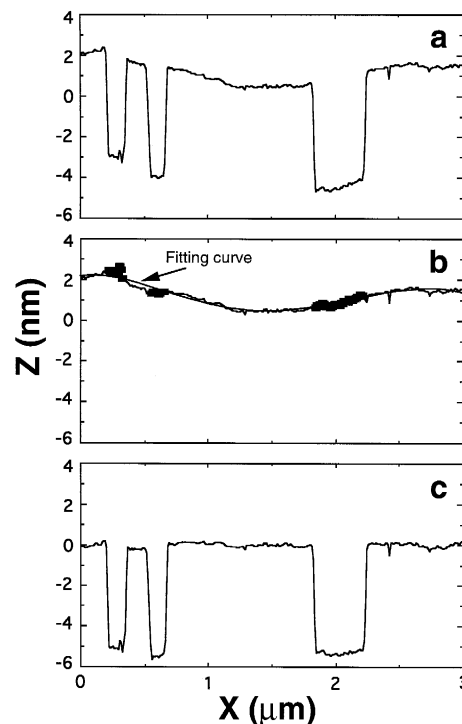

Fig. 2. A scanning line profile to demonstrate the method of how to determine the defect area coverage. Part a is the original scanning line. Part b is obtained by raising those points in the defects by a height of the thickness determined at the edge (5.3 nm in this case). The fitting curve in part b is a polynomial fit of power 5. Part c is obtained by subtracting the fitting curve from the original scanning line.

Rather, it is the result of some drifting in the electronics, as mentioned in the above. Moreover, this is true since we also observe similar modulation when imaging atomic flat mica surfaces at large scanning sizes. Such a drifting would not affect the determination of the defect coverage if areal measurements were carried out manually, since the edges of the defects are clearly defined. However, to count defect coverage automatically, the simplest method of defining a threshold value with points below the threshold belonging to defects may encounter difficulty. Yet, to analyze a large number of AFM images in a timely fashion, automatic determination of the defect coverage is essential. One remedy for this problem is to raise those data points in defect areas by the thickness determined from the edges, discarding a few points at the edges. This gives a smooth curve in which the slow modulation can be fitted to a polynomial (of power 5 in our case), as shown in Fig. 2b.

Subtracting the fitting curve from the scanning data, we obtain a flattened curve (Fig. 2c) in which the defect area can be determined automatically by counting those points below a threshold (-2 nm in this example). We exercised this procedure in analyzing all images in the present study. Note the bilayer thickness in these small defects is less than 6 nm. We often found that the thickness tends to be smaller for small defects. Two factors may contribute to this phenomenon. One is that the defects are too small to allow the tip to reach the substrate. The other is the presence of some surface contamination in the valley. We determine the bilayer thickness by the edges of large defects which in most cases were created by the scraping method, and the average of such determined thickness is 6 nm.

2.5. Characterization of lipid degradation

Some of our experiments lasted long time and lipid bilayers in some of our experiments were heated to higher temperatures several times. A natural question is whether lipids will degrade under our experimental conditions. The substrates in our experiments are small ($\approx 3 \times 5$ mm^2). This makes it very difficult to recover lipids from our specimens after the experiments because of the loss of most lipids on the substrates. However, it is reasonable to believe that the quality of lipids under our experiments can be characterized if we examine lipids from the same source under conditions similar to our lipid loss experiments. TLC was used for this purpose. For lipids in vesicular suspension, we did not detect any degradation when the suspension was allowed to stay at room temperature for over two months, nor did we detect any lipid degradation when the suspension was subjected to repeated heating to about 75°C for eight times. These results indicate that lipid degradation is not likely in our experiments.

3. Results

3.1. Structural features of the lipid-loss process

Fig. 3 summarizes our studies of the lipid-loss process of supported DPPC bilayers under six incubation temperatures. For each temperature, four repre-

sentative AFM images of the bilayer under different incubating times are shown. The top four images are examples at 75°C, in which many thinner domains are seen in Fig. 3 part I.b. Yet, in parts I.c and I.d, only bilayer defects are there. Thinner domains are also seen in experiments carried out at 65°C, 55°C and 45°C, as can be seen in Fig. 3 parts II.c, III.b, III.c, III.d and IV.c. In most cases, these domains were not present in original bilayers and disappeared after a certain period of time. Most original supported bilayers contain small natural defects, as can be seen in Fig. 3 (I.a–VI.a). Different defect coverages in original bilayers do not have any effect on the lipid-loss rate. These defects are too small to allow measurements of the bilayer thickness. Thus, tip-scraped defects are used to measure the bilayer thickness, which is about 6 nm, consistent with other studies [32]. The loss of lipid molecules increases the number and the area of bilayers defects. The shape of these defects, though, remains irregular in most circumstances. Some white spots seen in some images are debris scattered on the bilayer surface. The origin of these debris is not clear.

A striking feature appears in the lipid-loss process. We see many structural domains which are about 2 nm lower than the bilayer plane when the lipid-loss processes took place at 45°C and higher temperatures. Therefore, the thickness of these thinner domains is about 4 nm. The darkest areas are bilayer defects. The light gray regions are bilayers. The shaded regions with a contrast between the two extremes are the thinner domains. Most of these domains are in contact with some bilayer detects when initially appeared. These thinner domains fade away after increasing incubation, accompanying by increases in both the number and the area of bilayer defects. For the lipid-loss processes at room temperature and at 28°C, we did not detect any thinner domain. Generally, the lipid loss results in an initial increase in the number of bilayer defects. Gradually, bilayer defects become larger as the incubation time increases. For the lipid-loss processes at the higher temperatures, the thinner domains appear at earlier times. Later, these thinner domains fade away, replaced by larger bilayer defects. Usually, as more than 40% lipid molecules are lost, many bilayer defects are filled with small aggregates. Then, it becomes difficult to measure the surface coverage of defects, since some
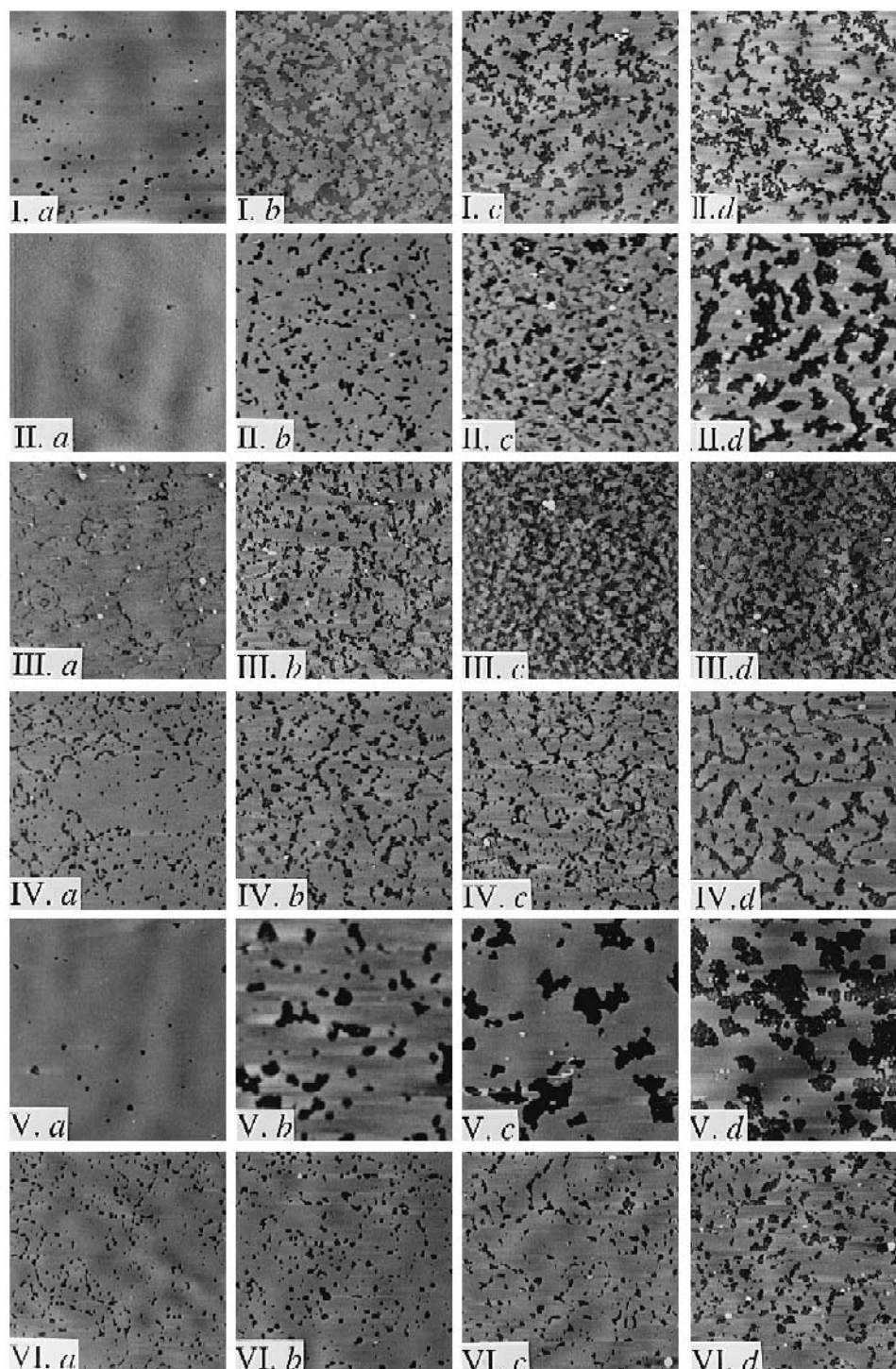
Fig. 3. Representative AFM images of the supported unilamellar bilayers under six lipid-loss incubation temperatures at different times. The leftmost images in all six groups are original bilayers. Other bilayers are: (I.b–d) incubating for 20 (b), 60 (c), and 110 (d) min respectively at 75°C; (II.b–d) incubating for 30 (b), 120 (c), and 180 (d) min respectively at 65°C; (III.b–d) incubating for 120 (b), 240 (c), and 420 (d) min respectively at 55°C; (IV.b–d) incubating for 90 (b), 180 (c), and 510 (d) min respectively at 45°C; (V.b–d) incubating for 1440 (b), 2880 (b), and 5400 (d) min respectively at 28°C; and (VI.b–d) incubating for 1440 (b), 5340 (c), and 10080 (d) min respectively at room temperature (23°C).

aggregates are not much lower than the level of the planar bilayer. When this happens, we stop our statistical analysis of the lipid-loss process.

3.2. The interdigitated domains

Fig. 4 shows two images in which the thinner domains are present. Here, the domains are induced during the lipid loss at 75°C. One intuitive explanation for these domains would be that they may be temporary monolayers as a result of the lipid-loss process. Since for supported monolayers the acyl chains are facing the solution, an adhesion force should exist because of the hydrophobic interaction between the hydrophobic AFM tip and the acyl chains [46]. However, in our experiments, the imaging is very stable on these domains without any adhesion force. Thus to attribute the observed domains as monolayers cannot reconcile with our experimental observations. Another explanation is to attribute these thinner domains as tilted bilayers. Whether this is possible can be analyzed be examining our experimental conditions. In our experiments, these domains were detected at room temperature after cooling down from high temperature. In all cases the bilayers stayed at room temperature for over 10 min before examined by the AFM, and that AFM imaging easily lasted for several hours. The lipids are in the gel phase at room temperature. Taking into account of a hydration layer and that the gel phase DPPC is tilted by 32° [35], the thickness of about 4 nm indicates that the tilting angle of the lipids should be larger than 65° if the thinner domains are of tilted bilayers. This would mean that the thinner domains we observed here

might be due to a new bilayer structure. This is unlikely the case, since bilayers of gel phase DPPC with such a large tilting angle has not been observed by any other method. A reasonable explanation is to attribute them as interdigitated domains as reported elsewhere in different studies [33], on the basis of the thickness of these domains, the lack of any adhesion force, and without any difficulty in stable imaging.

Our AFM images reveal that the interdigitated domains are mostly of small areas. These observations are different from the case of alcohol-induced lipid interdigitation in supported bilayers, in which extended areas of interdigitated domains were observed [33]. In particular, when initially detected, most interdigitated domains were in contact with some even smaller bilayer defects, as shown in Fig. 4a. This structural characteristic of interdigitated domains in our systems may provide essential clues about the origin of how the interdigitated domains are induced. Continuing the lipid-loss process results in the decrease of average sizes of the interdigitated domains, and some of the domains are no longer in contact with bilayer defects, as shown in Fig. 4b. We see the decrease in the area and the coverage of the interdigitated domains at the increase in the area of bilayer defects. The shape is also irregular for these interdigitated domains.

3.3. Statistics of the lipid-loss process

The lipid loss in our systems is characterized by the areal increase of bilayer defects. All bilayer defects are much smaller than the resolution limit with optical microscopy. With AFM, these defects are directly observed and their areas are measured. However, the nature of AFM imaging does not allow us to obtain the structure of a supported bilayer over a large area (limited by the scanning size and the linearity of the scanning tube). We thus need to characterize the lipid-loss process based on statistics by random sampling at different locations on the substrate. The areas of defects are measured to obtain their percentage coverage. For each sample under a certain incubation temperature, about ten AFM images were taken at different locations for each incubation time. For each incubation time, several samples are used to obtain more significant statistics.
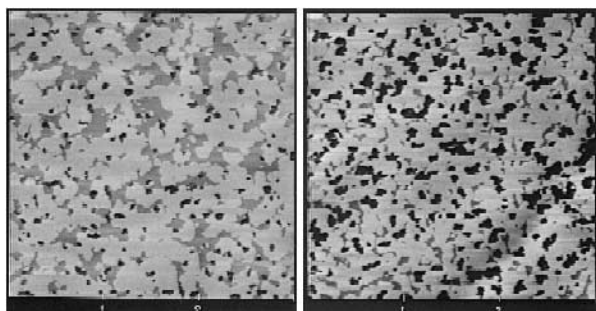
For the interdigitated domains, the unit surface

Fig. 4. Two representative AFM images of the interdigitated domains obtained at 75°C, where (a) was after incubating for 20 min and (b) was after incubating for 40 min.

area per lipid molecule is larger than that in a normal bilayer membrane. Thus, the total number of lipids for an interdigitated domain is smaller than that for a bilayer of the same area. To account for this effect, we used the method by Simon and McIntosh to calculate the loss of lipids due to the interdigitated domains [47]. The results of these calculations are added to the total loss of lipids to obtain an effective relative defect-area percentage. Briefly, the end of an interdigitated acyl chain is approximated as a half sphere of about 30 Å^2 according to Nagle and Wilkinson [48], which gives a projection area about
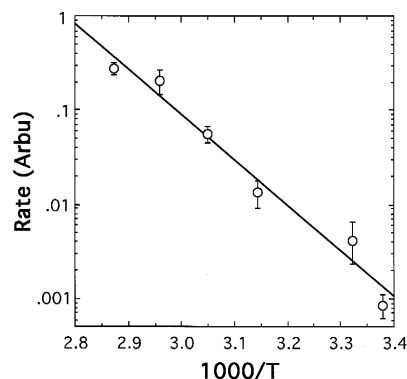
Fig. 6. Arrhenius plot of the rates of the lipid-loss process in supported DPPC bilayers. The line is a simple exponential fit, from which an activation energy of 37 kT is obtained.

15 Å^2. The projection area is what we can measure with AFM. For DPPC headgroup, the surface area has been determined by X-ray diffraction [49–51]. Taking the headgroup area as 47 Å^2 [50], two interdigitated acyl chains thus correspond to a surface area of about 64% of the surface area of a PC lipid headgroup in normal lipid bilayers.

We assume the lipid loss is a relaxational process, so that the amount of the lipid loss depends exponentially on the incubation time. Very slow rates of the lipid loss result in very long time constants. In the linear approximation, the slope in a plot of the relative defect-area percentage vs. incubation time is proportional to the lipid-loss rate at earlier times. Fig. 5 shows our results at six different lipid-exchange incubation temperatures. The linearity of these plots indicates very slow rates at all temperatures. The rate becomes slower at lower lipid-loss incubation temperatures. We note that the fitted slopes miss the origin. These fitting lines are the best fits, in which both the slopes and the constants of the linear fits also have standard deviations. Taking these deviations into account, we found that the missing of origins in our fittings is within the errors.

Fig. 6 is an Arrhenius plot of these rates at different temperatures. The error bars are standard deviations of the slopes in Fig. 5. From this plot we obtain an activation energy of 37 kT for the lipid-loss process in supported DPPC bilayers. This value is consistent with the activation energies of the lipid-exchange processes in vesicular systems [15–18].
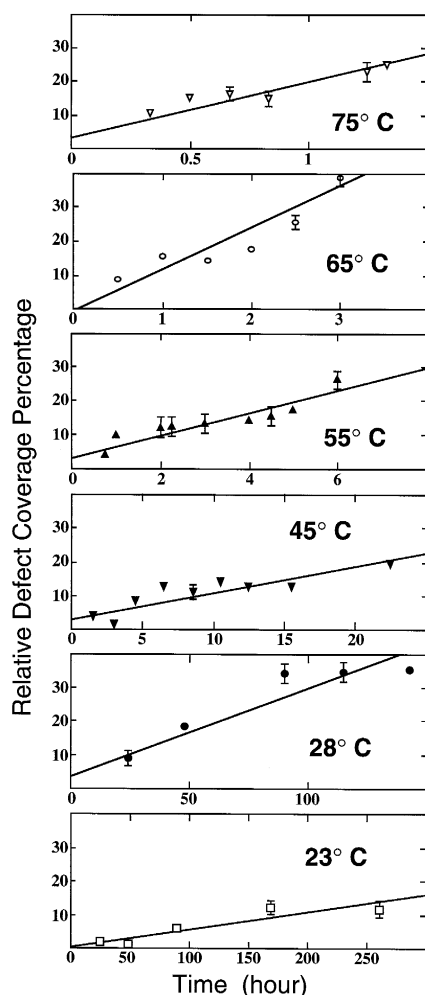

Fig. 5. Six plots of time vs. relative defect-area coverage are shown here. Each datum point was obtained by counting the relative defect-area coverage of about ten AFM images and averaging the results. The error bars are standard deviations. The lines are simple fits to the data.
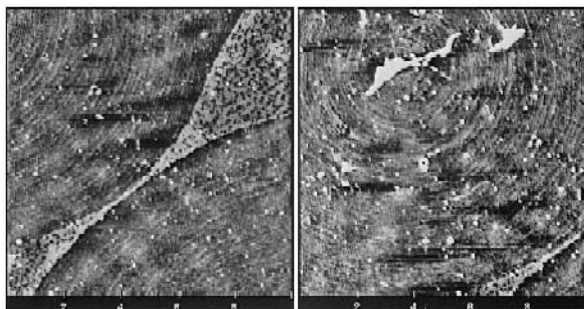
Fig. 7. Two AFM images are shown here to report an interesting structure observed while the lipid-loss process was at 65°C with the loss of most lipid molecules in the bilayer. Some circular structures of typical diameters about 10 μm can be seen. Some bilayer islands are seen at the edge of the circles.

3.4. Circular structures

Although our statistical analysis only proceeded to a relative defect-area increase of about 40%, we sometimes still followed the structural change of the bilayer while most lipid molecules leave the bilayer. Fig. 7 shows two examples. We see that some surface aggregates arrange into circular structures. Between these circular structures, there is a region containing many bilayer islands. The radius of the circular structure observed here is similar to that of the circular domains in monolayers at the air–water interface due to the phase separation of liquid-expanded phase from liquid-condensed phase [52,53]. Nagle has already pointed out that a bilayer is well characterized by a back-to-back pack of two weakly coupled monolayers [54–56]. Thus, it is possible that the observed circular structure here has a similar origin as that observed in the monolayers. At present, though, we do not have sufficient experimental evidence to support this conjecture. The phenomenon is still under study.

4. Discussion

Sackmann has shown that the driving force for the vesicle closure is very high, because of the large surface tension of bilayer membranes [57]. It is expected that the surface tension for supported bilayers should also be as large. Thus the appearance of bilayer defects in supported bilayers indicates that

there is a strong interaction between the substrate and the bilayer which stabilizes bilayer defects against the defect-closing force. Yet, experiments of neutron diffraction and deuterium-NMR suggest the existence of a hydration layer between the lower leaflet of a supported bilayer and the substrate [58,59]. AFM measurements of the bilayer thickness are consistent with the lamellar spacing in multilamellar bilayer stacks, in which a hydration layer exists between lipid bilayers [47], providing indirect evidence also in support of the existence of a hydration layer. However, water molecules in the hydration layer may be ordered, unlike those free water molecules in solution [60]. It is likely that the ordering of water molecules provides some kind of steric restriction on the movement of lipid molecules so that bilayer defects can exist in supported bilayers.

Although details of the interaction which stabilizes a supported bilayer against defects are not revealed in our studies, we can provide some features of this interaction by examining the structure of supported bilayers. It appears that most lipid molecules escape the bilayer around defect edges, evidenced by the fact that an increase of the defect area becomes more dominant in later times in the lipid-loss process. This phenomenon suggests that there may exist inhomogeneity in the bilayer so that the overall two-state scheme, that lipids in solution have one chemical potential and that lipids in the bilayer have another chemical potential, may be an oversimplification. A possible scenario is that the potential barrier for lipids to escape the bilayer may have a spatial gradient in the vicinity of defects, with a higher value farther away from the defect edge. Thus more lipids exit the bilayer around defect edges, resulting in an increase of defect areas at later times in the lipid-loss process.

The alcohol-induced interdigitated domains in supported PC bilayers are closely associated with the alcohol-induced interdigitated states in vesicular PC bilayers [33], so that the mechanism of the driving force of the lipid interdigitation in the former is mostly understood through extensive studies of the latter [47,61–63]. However, in our case, the system under study does not have any direct analogy with situations of vesicular bilayers. Our experimental results may provide some clues for rational explanations of the observations in the present study. For lipid bilayers, the boundary of any opening creates a

line tension which drives the closure of the opening [57]. This driving force should then apply an additional pressure to lipid molecules around defects, and the additional pressure may be sufficient to cause the bilayer interdigitation. For lipid bilayers, the surface tension is about 65 mM/m [56,64], and the typical bilayer thickness is about 4 nm [47]. These values give a closure pressure of about 160 bar at the boundary of bilayer defects. Some domains, although very rare, are not in contact with any apparent defect. It is possible that an initial defect is so small that the expansion of the induced interdigitated domain closes the defect.

The disappearance of interdigitated domains indicates that these domains are probably metastable intermediate states. Furthermore, the lack of any interdigitated domain at low temperatures indicates that interdigitated domains may be induced only when the lipid-loss rate is larger than a threshold value. The actual lipid-loss rates, on the other hand, are extremely slow. For example, if assuming a simple exponential decaying process, the percentage lipid loss being still approximately linear for more than 10 days indicates an even longer time constant at room temperature. At 75°C, the time constant is still of order hours (see Fig. 5). Although the activation energy determined from the Arrhenius plot is consistent with those determined from vesicular bilayers, the rates of the lipid loss, and thus of the lipid exchange, are much slower. Therefore, the behavior of supported bilayers is similar to that of vesicular bilayers in some aspects, and is distinct in other aspects.

In summary, our study shows that typical structural characteristics of the lipid-loss process are the creation and growth of bilayer defects accompanying, at high temperature in most cases, the induction of small interdigitated domains. Our results also demonstrate the power of in situ AFM in combining structural studies with thermodynamic characterizations in the research of membrane biophysics.

Acknowledgements

References

[1] Gennis, R.B. (1994) Biomembranes, Molecular Structure and Function, Springer-Verlag, New York.

[2] Narahashi, T. (ed.) (1994) Ion Channels of Excitable Cells, Academic Press, San Diego.

[3] Wallach, D.F.H. (1987) Fundamentals of Receptor Molecular Biology, pp. 149–181, Marcel Dekker, New York and Basel.

[4] Yeagle, P. (1993) The Membranes of Cells, 2nd edn., Academic Press, Orlando.

[5] Cevc, G. and Marsh, D. (1987) Phospholipid Bilayers: Physical Properties and Model, Wiley, New York.

[6] Seelig, J. and Seelig, A. (1980) Q. Rev. Biophys. 13, 19–61.

[7] Bergelson, L.D. (1988) in Biomembranes, Basic and Medical Research (Benga, G.H. and Tager, J.M., eds.), pp. 1–12, Springer-Verlag, Berlin.

[8] Sackmann, E. (1983) in Biophysics (Hoppe, W., Lohman, W., Markl, H. and Ziegler, H., eds.), pp. 425–430, Springer-Verlag, Berlin.

[9] Silver, B.L. (1985) The Physical Chemistry of Membranes, an Introduction to the Structure and Dynamics of Biological Membranes, Allen and Unwin, Boston.

[10] Starzak, M.E. (1984) The Physical Chemistry of Membranes, Academic Press, Orlando.

[11] Israelachivili, J.N., Marcelja, S. and Horn, R.G. (1980) Q. Rev. Biophys. 13, 121–200.

[12] De Kruijff, B., Van Den Besselaar, A.M.H.P., Cullis, P.R., Van Den Bosch, H. and Van Deenen. L.L.M. (1978) Biochim. Biophys. Acta 514, 1–8.

[13] Frank, A., Barenholz, Y., Lichtenberg, D. and Thompson, T.E. (1983) Biochemistry 22, 5647–5651.

[14] Kremer, J.M.H., Kops-Werkhoven, M.M., Pathmamanoharan, C., Gijzeman, O.L.J. and Wiersema, P.H. (1977) Biochim. Biophys. Acta 471, 177–188.

[15] McLean, L.R. and Phillips, M.C. (1981) Biochemistry 20, 2893–2900.

[16] McLean, L.R. and Phillips, M.C. (1982) Biochemistry 21, 4053–4059.

[17] Roseman, M.A. and Thompson, T.E. (1980) Biochemistry 19, 439–444.

[18] Wimley, W.C. and Thompson, T.E. (1990) Biochemistry 29, 1296–1303.

[19] Zilversmit, D.B. and Hughes, M.E. (1977) Biochim. Biophys. Acta 469, 99–110.

[20] Alberts, B., Bray, D., Lewis, J., Raff, M., Roberts, K. and Watson, J.D. (1989) Molecular Biology of the Cell, Garland Publishing, New York and London.

[21] Darnell, J., Lodish, H. and Baltimore, D. (1990) Molecular Cell Biology, Scientific American Books, New York.

[22] Sackmann, E. (1996) Science 271, 43–48.

[23] Brain, A.A. and McConnell, H.M. (1984) Proc. Natl. Acad. Sci. USA 81, 6159–6163.

[24] McConnell, H.M., Watts, T.H, Weis, R.M. and Brian, A.A. (1986) Biochim. Biophys. Acta 864, 95–106.

[25] Hsieh, H.V., Poglitsch, C.L. and Thompson, N.L. (1992) Biochemistry 31, 11562–11566.

[26] Poglitsch, C.L. and Thompson, N.L. (1990) Biochemistry 29, 248–254.

[27] Pearce, K.H., Hiskey, R.G. and Thompson, N.L. (1992) Biochemistry 31, 5983–5995.

[28] Tendian, S.W., Lentz, B.R. and Thompson, N.L. (1991) Biochemistry 30, 10991–10999.

[29] Drake, B., Prater, C.B., Weisenhorn, A.L., Gould, S.A.C., Albrecht, T.R., Quate, C.F., Cannell, D.S., Hansma, H.G. and Hansma, P.K. (1989) Science 243, 1586–1589.

[30] Hansma, H.G., Gould, S.A.C., Hansma, P.K., Gaub, H.E., Longo, M.L. and Zasadzinski, J.A.N. (1991) Langmuir 7, 1051–1054.

[31] Hui, S.W., Viswanathan, R., Zasadzinski, J.A.N. and Israelachvili, J.N. (1995) Biophys. J. 68, 171–178.

[32] Mou, J., Yang, J. and Shao, Z. (1994) Biochemistry 33, 4439–4443.

[33] Mou, J., Yang, J., Huang, C. and Shao, Z. (1994) Biochemistry 33, 9981–9985.

[34] Weisenhorn, A.L., Egger, M., Ohnesorge, F., Gould, S.A.C., Heyn, S.-P., Hansma, H.G., Sinsheimer, R.L., Gaub, H.E. and Hansma, P.K. (1991) Langmuir 7, 8–12.

[35] Yang, J., Tamm, L.K., Tillack, T.W. and Shao, Z. (1993) J. Mol. Biol. 229, 286–290.

[36] Zasadzinski, J.A.N., Helm, C.A., Longo, M.L., Weisenhorn, A.L., Gould, S.A.C. and Hansma P.K. (1991) Biophys. J. 59, 755–760.

[37] Butt, H.-J., Downing, K.H. and Hansma, P.K. (1990) Biophys. J. 58, 1473–1480.

[38] Hoh, J.H., Sosinsky, G.E., Revel, J.-P. and Hansma, P.K. (1993) Biophys. J. 65, 149–163.

[39] Karrasch, S., Hegerl, R., Hoh, J.H., Baumeister, W. and Engel, A. (1994) Proc. Natl. Acad. Sci. USA 91, 836–838.

[40] Mou, J., Yang, J. and Shao, Z. (1995) J. Mol. Biol. 248, 507–512.

[41] Schabert, F.A., Henn, C. and Engel, A. (1995) Science 268, 92–94.

[42] Shao, Z. and Yang, J. (1995) Q. Rev. Biophys. 28, 195–251.

[43] Yang, J. and Shao, Z. (1995) Micron 26, 35–49.

[44] Boni, L.T., Minchey, S.R., Perkins, W.R., Ahl, P.L., Slater, J.L., Tate, M.W., Gruner, S.M. and Janoff, A.S. (1993) Biochim. Biophys. Acta 1146, 247–257.

[45] Kantor, H.L., Mabrey, S., Prestegard, J.H. and Sturtevant, J.M. (1977) Biochim. Biophys. Acta 466, 402–410.

[46] O'Shea, S.J., Welland, M.E. and Rayment, T. (1992) Appl. Phys. Lett. 60, 2356–2358.

[47] Simon, S.A, and McIntosh, T.J. (1984) Biochim. Biophys. Acta 773, 169–172.

[48] Nagle, J.F. and Wilkinson, D.A. (1978) Biophys. J. 23, 159–175.

[49] Lis, L.J., McAlister, M., Fuller, N., Rand, R.P and Parsegian, V.A. (1982) Biophys. J. 37, 657–666.

[50] Tristram-Nagle, S., Zhang, R., Suter, R.M., Worthington, C.R., Sun, W.-J. and Nagle, J.F. (1993) Biophys. J. 64, 1097–1109.

[51] Pearson R.H. and Pascher, I. (1979) Nature 281, 499–501.

[52] Losche, M. and Mohwald, H. (1984) Eur. Biophys. J. 11, 35–42.

[53] McConnell, H.M., Tamm, L.K. and Weis, R.M. (1984) Proc. Natl. Acad. Sci. USA 81, 3249–3253.

[54] Nagle, J.F. (1975) J. Chem. Phys. 63, 1255–1261.

[55] Nagle, J.F. (1976) J. Membr. Biol. 27, 233–250.

[56] Nagle, J.F. (1986) Faraday Discuss. Chem. Soc. 81, 151–162.

[57] Sackmann, E. (1994) FEBS Lett. 346, 3–16.

[58] Bayerl, T.M. and Bloom, M. (1990) Biophys. J. 58, 357–362.

[59] Johnson, S.J., Bayerl, T.M., McDermott, D.C., Adam, G.W., Rennie, A.R., Thomas, R.K. and Sackmann, E. (1991) Biophys. J. 59, 289–294.

[60] McIntosh, T.J. and Simon, S.A. (1994) Annu. Rev. Biophys. Biomol. Struct. 23, 27–51.

[61] Rowe, E.S. (1987) Biochemistry 26, 46–51.

[62] Slater, J.L. and Huang, C. (1988) Prog. Lipid Res. 27, 325–359.

[63] Yamazaki, M., Miyazu, M., Asano, T., Yuba, A. and Kume, N. (1994) Biophys. J. 66, 729–733.

[64] Evans, E.A. and Waugh, R. (1977) J. Colloid Interface Sci. 60, 286–298.